Robotica (2002) volume 20, pp. 519–528. © 2002 Cambridge University Press
DOI: 10.1017/S0263574702004265 Printed in the United Kingdom

Two-time scale controller design for a high speed planar parallel manipulator with structural flexibility

Bongsoo Kang, Benny Yeung and James K. Mills*

Department of Mechanical and Industrial Engineering, University of Toronto, 5 King's College Road, Toronto, Ontario (Canada) M5S 3G8

(Received in Final Form: March 20, 2002)

SUMMARY

Planar parallel manipulators, with potential applications in high speed, high acceleration tasks such as electronic component placement, would be subject to mechanical vibration due to high inertial forces acting on the linkages and other components. To achieve high throughput capability, such motion induced vibration would have to be damped quickly, to reduce settling time of the platform position and orientation. This paper develops a two-time scale dynamic model of a three-degree-of-freedom planar parallel manipulator with structurally flexible linkages. Based on the two-time scale model, a composite controller, consisting of a computed torque controller for the slow time-scale or rigid body subsystem dynamics, and a linear-quadratic state-feedback regulator for the fast time-scale flexible dynamic subsystem, is designed. Simulation results show that the composite control scheme permits the parallel manipulator platform to follow a given desired trajectory, while damping structural vibration arising due to excitation from inertial forces.

KEYWORDS: High speed; Planar parallel manipulator; Structural flexibility; Composite control.

1. INTRODUCTION

A high-speed pick-and-place positioning mechanism is an indispensable element in various industrial fields, especially in electronic manufacturing, where small product size and short assembly times characterize the manufacturing process. Serial architecure manipulators, such as X-Y tables or gantry robots, designed for these tasks, are characterized by the simplicity of their control systems, since each axis can be treated as an independent unit. However, these configurations limit high speed and acceleration performance, since the inertia of distal axis hardware, including actuators, has a significant influence on the performance of supporting axes.

The planar parallel manipulator[1–3] architecture provides an alternative design to serial mechanisms, and with proper selection of active joints, can result in low moving inertia independent of the mass of actuators. This reduced mass of moving components permits high acceleration and high payload capacity. The mechanism design provides high mechanical rigidity leading to precise manipulation. However, although there are a number of positive attributes of planar parallel mechanisms, the design of a planar parallel manipulator is made more complex due to its small workspace and associated singularities. Hence, considerable research has focused on kinematic analysis[4] and singularity characterization of these devices.[5,6] Planar parallel manipulators typically consist of three closed chains and a moving platform. Depending on whether revolute or prismatic joints, denoted by R and P respectively, are used in one chain, these devices are classified as RRR, RPR, PPP, etc.

A number of approaches to develop equations of motion of planar parallel manipulators have been presented in the literature. Multiple closed-loop chains in a parallel manipulator result in dynamic equations of motion which include reaction forces between all moving components, when developed using the Newton-Euler method,[7] or constraint equations, when developed using the Lagrangian method.[8] The electronics fabrication industry demands high-speed, high acceleration placement machines, with correspondingly lightweight linkages, hence, these linkages deform under high inertia forces. As a result, modeling structurally flexible linkages, which make up closed-loop kinematic chains of parallel manipulators, has been the focus of substantial attention in the literature.[9–11]

In this paper, a *P*RR type planar parallel manipulator configuration is introduced. Based on the dynamic model of the planar parallel manipulator derived in reference [11], a two time scale dynamic model is developed. Due to the presence of multiple closed-loop chains, parallel manipulators are subject to a number of kinematic constraints. In the development of the two-time scale model, two-time scale model reduction is first performed, to separate slow time-scale rigid-body motions from fast time-scale inertial force induced vibration motion. Initially proposed by Siciliano and Book,[12] the composite control approach was first applied to a serial two-link manipulator[13] and to serial manipulators during constrained motion.[14,15] Utilizing these developments, a composite controller, consisting of a trajectory follower for the slow time-scale subsystem, and a damper for the fast time-scale subsystem, is designed. With linkages of the planar parallel manipulator modeled with structural flexibility, simulations are performed to verify the two-time scale dynamic model and demonstrate feasibility

* Corresponding Author: Professor James K. Mills, Department of Mechanical and Industrial Engineering, University of Toronto, 5 King's College Road, Toronto, Ontario (Canada) M5S 3G8.
mills@mie.utoronto.ca

https://doi.org/10.1017/S0263574702004265 Published online by Cambridge University Press

of the composite control approach to planar parallel manipulators.

The main purpose for investigation into the use of two time-scale controllers is to exploit the inherent advantage of this approach over active damping control approaches, which require the use of additional sensors and actuators to damp structural vibration. Such active vibration control approaches require the use of additional actuators such as piezoelectric material, lead zirconium titanate (PZT), to damp vibration. In sharp contrast to these approaches, two time-scale controllers do not require additional sensors and actuators to damp vibration. Hence, this approach results in an advantage in cost and complexity over active damping control approaches.

This paper is organized as follows. Section 2 describes the architecture of the planar parallel manipulator and Section 3 introduces the two-time scale model. The composite control scheme is given in Section 4 and simulation results are given in Section 5. Finally, conclusions are given in Section 6.

2. ARCHITECTURE OF PLANAR PARALLEL MANIPULATOR

The architecture of the planar parallel mechanism is illustrated in Figure 1. The moving platform exhibits translation and rotational motion. The platform is shown as a regular triangular shape with revolute joints on each vertex. Three intermediate linkages between the moving platform and sliders convert actuating forces into movements of the platform. Both ends of the intermediate linkage are composed of non-actuated revolute joints. The motion of the sliders can be achieved with either a ball-screw mechanism driven by a rotary motor or a linear motor.

The planar manipulator is categorized as a *P*RR type, because a closed chain consists of a prismatic joint and two consecutive revolute joints, beginning from the prismatic joint of the slider to the revolute joint between the linkage and the platform. In contrast to the well-known Stewart-Gough platform,[16] the driving actuators are stationary, as shown in Figure 1, hence are not included in the total inertia of moving components since the actuators are attached to the prismatic joints. The following section presents the twotime scale model of the planar parallel manipulator, in order to investigate not only vibration of the platform due to structural flexibility, but also performance of the composite controller in vibration attenuation.

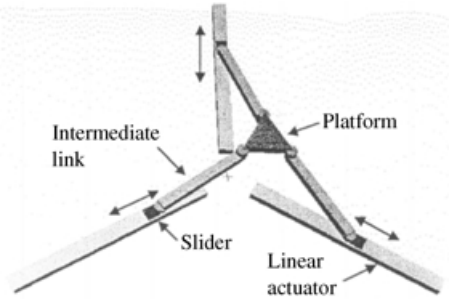


Fig. 1. Configuration of planar parallel manipulator with motion of slides indicated.

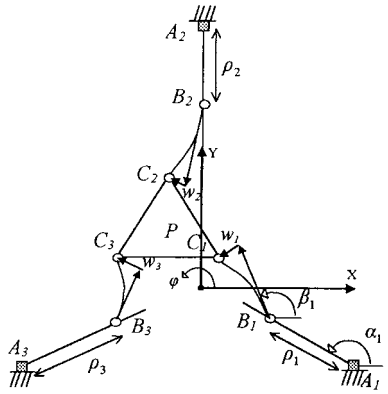


Fig. 2. Schematic illustrating the coordinates of the parallel manipulator. Note the linkages B_iC_i, $i=1,2,3$ are shown with exaggerated deformations.

3. TWO TIME-SCALE MODEL

Generalized coordinates for the planar manipulator are assigned, as shown in Figure 2. The position and orientation (pose) of the platform, at its mass center, *P*, with respect to a reference frame X-Y, shown in Figure 2, is defined as

$$\boldsymbol{X}_P \equiv [x_P,\ y_P,\ \phi]^T \in \Re^3 \tag{1}$$

The origin of the reference frame X-Y, is placed at the point where imaginary extended lines of three linear actuators intersect, as shown in Figure 2. The displacement of the sliders from their origin, A_i, to B_i, is expressed as

$$\boldsymbol{\rho} \equiv [\rho_1,\ \rho_2,\ \rho_3]^T \in \Re^3 \tag{2}$$

Finding positions of the sliders corresponds to an inverse kinematic solution when the pose of the platform is given. Since there are two possible inverse kinematic solutions for each chain, the manipulator can take on a maximum of eight configurations for a single set of coordinates of the platform. β_i is defined as the angle between the X-axis of the fixed frame and the i^{th} link at B_i and α_i is the constant angle between the X-axis and the i^{th} linear actuator. Each vertex of the platform is denoted as C_i. Three linkages, including associated coordinates, are numbered with a subscript, i, starting from the lower right link in a counterclockwise direction.

The three linkages are assumed to exhibit structural flexibility, hence the shape of the linkages, under high acceleration, are shown deformed, in Figure 2. The lateral deformation of i^{th} linkage from its undeformed distal end, C_i, is denoted as w_i. Out of X-Y plane deformations are not considered in this paper. Utilizing an assumed modes model,[17] these lateral flexible deforrnations are expressed as follows;

$$w_i(\xi,t) = \sum_{j=1}^{r} \eta(t)_{ij}\psi_j(\xi) \qquad i=1,2,3 \tag{3}$$

where: ξ is a non-dimensional coordinate along the link, $0 \le \xi \le 1$.

The subscript, j, implies the j^{th} vibration mode and r represents a finite number of assumed modes. Assuming that both ends of the link exhibit pinned-free motion at B_i

https://doi.org/10.1017/S0263574720004265 Published online by Cambridge University Press

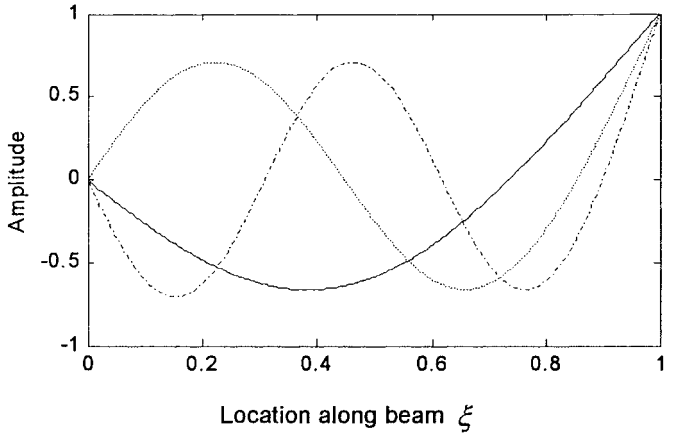


Fig. 3. Amplitude of first three mode shapes of the beam vs location along beam ξ
(solid line: first mode, dotted line: second mode, dash-dot line: third mode).

and C_i respectively, normalized shape functions, satisfying these boundary conditions, are selected as:

$$\psi_j(\xi)=\frac{1}{2\sin(\gamma_j)}\left[\sin(\gamma_j\xi)+\frac{\sin(\gamma_j)}{\sinh(\gamma_j)}\sinh(\gamma_\xi\xi)\right] \quad (4)$$

where: $\gamma_j=(j+0.25)\pi l \quad j=1,2,\ldots,r$

$l=$length of link.

Figure 3 shows the first three shape functions expressed in Equation (4).

The generalized coordinates ofthe platform are denoted, in vector form as:

$$\boldsymbol{X}\equiv[\boldsymbol{\rho},\ \boldsymbol{\beta},\ \boldsymbol{X_P},\ \boldsymbol{\eta}]^T\in\Re^{9+3r} \quad (5)$$

where: $\boldsymbol{\beta}\equiv[\beta_1,\ \beta_2,\ \beta_3]^T\in\Re^3$

$$\boldsymbol{\eta}\equiv[\eta_{11}\ \cdots\ \eta_{1r}\quad \eta_{21}\ \cdots\ \eta_{2r}\quad \eta_{31}\ \cdots\ \eta_{3r}]^T\in\Re^{3r}$$

Using the Lagrangian equation of the first type, with generalized coordinates defined previously, the equations of motion of the planar parallel manipulator are complete with a total of $9+3r$ equations,[11] given below;

$$\begin{bmatrix}\boldsymbol{M}_{11} & \boldsymbol{M}_{12} & \mathbf{0} & \boldsymbol{M}_{14}\\ \boldsymbol{M}_{12}^T & \boldsymbol{M}_{22} & \mathbf{0} & \boldsymbol{M}_{24}\\ \mathbf{0} & \mathbf{0} & \boldsymbol{M}^{33} & \mathbf{0}\\ \boldsymbol{M}_{14}^T & \boldsymbol{M}_{24}^T & \mathbf{0} & \boldsymbol{M}_{44}\end{bmatrix}\begin{bmatrix}\ddot{\boldsymbol{\rho}}\\ \ddot{\boldsymbol{\beta}}\\ \ddot{\boldsymbol{X}}_P\\ \ddot{\boldsymbol{\eta}}\end{bmatrix}+\begin{bmatrix}\boldsymbol{V}_1\\ \boldsymbol{V}_2\\ \mathbf{0}\\ \boldsymbol{V}_4\end{bmatrix}$$

$$+\begin{bmatrix}\mathbf{0} & \mathbf{0} & \mathbf{0} & \mathbf{0}\\ \mathbf{0} & \mathbf{0} & \mathbf{0} & \mathbf{0}\\ \mathbf{0} & \mathbf{0} & \mathbf{0} & \mathbf{0}\\ \mathbf{0} & \mathbf{0} & \mathbf{0} & \boldsymbol{K}\end{bmatrix}\begin{bmatrix}\boldsymbol{\rho}\\ \boldsymbol{\beta}\\ \boldsymbol{X}_P\\ \boldsymbol{\eta}\end{bmatrix}=\begin{bmatrix}\boldsymbol{U}\\ \cdots\\ \mathbf{0}\end{bmatrix}+\begin{bmatrix}\boldsymbol{J}_{\Gamma1}\\ \boldsymbol{J}_{\Gamma2}\\ \boldsymbol{J}_{\Gamma3}\\ \boldsymbol{J}_{\Gamma4}\end{bmatrix}\boldsymbol{\lambda} \quad (6)$$

where: $\boldsymbol{M}_{11}\in\Re^{3\times3}$, $\boldsymbol{M}_{12}\in\Re^{3\times3}$, $\boldsymbol{M}_{14}\in\Re^{3\times3r}$, $\boldsymbol{M}_{22}\in\Re^{3\times3}$, $\boldsymbol{M}_{24}\in\Re^{3\times3r}$, $\boldsymbol{M}_{33}\in\Re^{3\times3}$, $\boldsymbol{M}_{44}\in\Re^{3\times3r}\equiv$ inertia matrices

$\boldsymbol{V}_1\in\Re^3$, $\boldsymbol{V}_2\in\Re^3$, $\boldsymbol{V}_4\in\Re^{3r}\equiv$ vectors of Coriolis and centrifugal terms

$\boldsymbol{K}\in\Re^{3r\times3r}\equiv$ stiffness matrix of the linkages

$\boldsymbol{\lambda}\in\Re^6\equiv$ vector of Lagrange multipliers

$\boldsymbol{J}_{\Gamma1}\in\Re^{3\times6}$, $\boldsymbol{J}_{\Gamma2}\in\Re^{3\times6}$, $\boldsymbol{J}_{\Gamma3}\in\Re^{3\times6}$, $\boldsymbol{J}_{\Gamma4}\in\Re^{3r\times6}\equiv$ partial derivatives of constraint equations with respect to corresponding generalized coordinates

$\boldsymbol{U}\equiv[u_1\ u_2\ u_3\ 0\ \cdots\ 0]^T\in\Re^9$, vector of control inputs

Except for $\boldsymbol{M}_{12}$ and $\boldsymbol{M}_{14}$, in which the matrix coefficients vary with the configuration of the manipulator, i.e. $\boldsymbol{X}_P$, the remaining mass matrices and stiffness matrix are time-invariant. The partial derivative, $\boldsymbol{J}_{\Gamma2}$, $\boldsymbol{J}_{\Gamma3}$, $\boldsymbol{J}_{\Gamma4}$ depend on the flexible variable, $\boldsymbol{\eta}$, as well as $\boldsymbol{X}_P$, while $\boldsymbol{J}_{\Gamma1}$ is time-invariant. Detailed expressions of each component in the above are given in the Appendix.

Since the inertia matrix is symmetric and positive definite, it can be inverted and its inverse is denoted by $\boldsymbol{H}$ given as:

$$\boldsymbol{H}\equiv\begin{bmatrix}\boldsymbol{H}_{11} & \boldsymbol{H}_{12}\\ \boldsymbol{H}_{21} & \boldsymbol{H}_{22}\end{bmatrix}\equiv\begin{bmatrix}\boldsymbol{M}_{11} & \boldsymbol{M}_{12} & \mathbf{0} & \boldsymbol{M}_{14}\\ \boldsymbol{M}_{12}^T & \boldsymbol{M}_{22} & \mathbf{0} & \boldsymbol{M}_{24}\\ \mathbf{0} & \mathbf{0} & \boldsymbol{M}_{33} & \mathbf{0}\\ \boldsymbol{M}_{14}^T & \boldsymbol{M}_{24}^T & \mathbf{0} & \boldsymbol{M}_{44}\end{bmatrix}^{-1} \quad (7)$$

where $\boldsymbol{H}_{11}\in\Re^{9\times9}$, $\boldsymbol{H}_{12}\in\Re^{9\times3r}$, $\boldsymbol{H}_{21}\in\Re^{3r\times9}$, and $\boldsymbol{H}_{22}\in\Re^{3r\times3r}$.

Redefining the generalized coordinates as $\boldsymbol{q}\equiv[\boldsymbol{\rho},\ \boldsymbol{\beta},\ \boldsymbol{X}_P]^T\in\Re^9$, Equation (6) becomes

$$\begin{bmatrix}\ddot{\mathbf{q}}\\ \ddot{\boldsymbol{\eta}}\end{bmatrix}=\begin{bmatrix}\mathbf{H}_{11} & \mathbf{H}_{12}\\ \mathbf{H}_{21} & \mathbf{H}_{22}\end{bmatrix}\left\{-\begin{bmatrix}\mathbf{f}_1(\mathbf{q},\dot{\mathbf{q}})\\ \mathbf{f}_2(\mathbf{q},\dot{\mathbf{q}})\end{bmatrix}-\begin{bmatrix}\mathbf{g}_1(\mathbf{q},\dot{\mathbf{q}},\boldsymbol{\eta},\dot{\boldsymbol{\eta}})\\ \mathbf{0}\end{bmatrix}\right.$$

$$\left.-\begin{bmatrix}\mathbf{0}\\ \mathbf{K}\boldsymbol{\eta}\end{bmatrix}+\begin{bmatrix}\mathbf{U}\\ \mathbf{0}\end{bmatrix}+\begin{bmatrix}\mathbf{J}^1\\ \mathbf{J}_2\end{bmatrix}\boldsymbol{\lambda}\right\} \quad (8)$$

where:

$$\boldsymbol{J}_1\equiv\begin{bmatrix}\boldsymbol{J}_{\Gamma1}\\ \boldsymbol{J}_{\Gamma2}\\ \boldsymbol{J}_{\Gamma3}\end{bmatrix}\in\Re^9$$

$\boldsymbol{J}_2\equiv\boldsymbol{J}_{\Gamma4}\in\Re^{3r}$

$\boldsymbol{g}_1\in\Re^9\equiv$ vector containing velocity terms related to $\dot{\boldsymbol{\eta}}$ amongst $\boldsymbol{V}_1$, $\boldsymbol{V}_2$, $\boldsymbol{V}_4$

$\boldsymbol{f}_1\in\Re^9$, $\boldsymbol{f}_2\in\Re^{3r}\equiv$ velocity terms independent of $\dot{\boldsymbol{\eta}}$ amongst $\boldsymbol{V}_1$, $\boldsymbol{V}_2$, $\boldsymbol{V}_4$

https://doi.org/10.1017/S0263574720004265 Published online by Cambridge University Press

Utilizing the singular perturbation approach found in reference [12], a new variable, considered as an elastic force, is defined as

$$z \equiv \frac{\tilde{K}\eta}{\mu}, \text{ elastic force, } z \in \Re^{3r} \tag{9}$$

where: $\tilde{K} \equiv \mu K$, scaled stiffness matrix, $\tilde{K} \in \Re^{3r \times 3r}$

$\mu \equiv$ reciprocal of the smallest diagonal element of the stiffness matrix, K

Substitution of the variables introduced in Equation (9) into Equation (8), leads to a two-time scale form, where for notational simplicity, arguments of variables are not shown;

$$\ddot{q} = -H_{11} f_1 - H_{12} f_2 - H_{11} g_1 - H_{12} z + H_{11} U + H_{11} J_1 \lambda + H_{12} J_2 \lambda \tag{10}$$

$$\mu \tilde{K}^{-1} \ddot{z} = -H_{21} f_1 - H_{22} f_2 - H_{21} g_1 - H_{22} z + H_{21} U + H_{21} J_1 \lambda + H_{22} J_2 \lambda \tag{11}$$

For a given configuration of the manipulator, as μ approaches zero, the system exhibits only rigid-body motions, since as $\mu \rightarrow 0$, the stiffness matrix approaches infinity. Flexible dynamics of the system can be separated from rigid-body dynamics of the system as long as μ is small.[13]

When μ is set to be zero in Equation (11), since g_1 is zero,[12] z is given by

$$z_s = H_{22,s}^{-1}(H_{21,s}(-f_{1,s} + U_s + J_{1,s}\lambda s) - f_{2,s} + J_{2,s}\lambda_s \tag{12}$$

where subscript "s" indicates that corresponding quantities are computed in the slow time-scale, i.e. $\mu = 0$. Using the Equation (12), Equation (10) is rewritten as:

$$\ddot{q}_s = M_s^{-1}(-f_{1,s} + U_s + J_{1,s}\lambda_s) \tag{13}$$

where: $M_s^{-1} = H_{11,s} - H_{12,s} H_{22,s}^{-1} H_{21,s}$.

Equation (13) represents the slow time-scale system. Setting $\mu = 0$ results in a reduction of the order of Equation (10), (11) from $9 + 3r$ to 9.

In order to formulate the fast time-scale system, fast time-scale states are defined as follows;

$$z_f \equiv z - z_s, \; z_f \in \Re^{3r} \tag{14}$$

$$U_f \equiv U - U_s, \; U_f \in \Re^{9} \tag{15}$$

Using the above fast time-scale variable definitions, Equation (11) can be transformed to the following;

$$z_f'' = \tilde{K} H_{22,s} z_f + \tilde{K} H_{21,s} U_f \tag{16}$$

where: $(\cdot)''$ denotes $\frac{d^2(\cdot)}{d\tau^2}$ where $\tau \equiv \frac{t}{\sqrt{\mu}}$, the fast time scale.

The fast time-scale motion, described by Equation (16), is a linear time-invariant system, in which all system coefficients are calculated in the slow time-scale.

4. COMPOSITE CONTROL SCHEME

Based on the two time-scale model described in the previous section, controllers for the slow and fast time-scale subsystems can be designed separately, to meet objectives of each respective subsystem. The slow time-scale controller should provide a trajectory tracking capability for the platform, while the fast time-scale controller should be designed to damp out vibration of flexible linkages resulting from rapid rigid body motion of the manipulator. The computed torque control method,[18] given below, is applied to the slow time-scale subsystem representing the rigid-body motion of the platform:

$$U_s = \hat{M}_s \ddot{q}_c + \hat{f}_{1,s} - J_{1,s} \lambda_s \tag{17}$$

where: $\ddot{q}_c = \ddot{q}_d + K_{sp}(q_d - q) + K_{sd}(\dot{q}_d - \dot{q})$,

$\hat{M}_s \equiv$ estimated value of the mass matrix M_s, $\hat{M}_s \in \Re^{9 \times 9}$

$\hat{f}_{1,s} \equiv$ estimated velocity terms independent of $\dot{\eta}$ amongst V_1, V_2, V_4, $\hat{f}_{1,s} \in \Re^9$

$\ddot{q}_d \equiv$ desired acceleration vector of $\ddot{q}$, $\ddot{q}_d \in \Re^9$

$\dot{q}_d \equiv$ desired velocity vector of $\dot{q}$, $\dot{q}_d \in \Re^9$

$q_d \equiv$ desired position vector of q, $q_d \in \Re^9$

$K_{sp} \equiv$ proportional feedback gain matrix for the slow time-scale subsystem, $K_{sp} \in \Re^{9 \times 9}$

$K_{sd} \equiv$ derivative feedback gain matrix for the slow time-scale subsystem, $K_{sd} \in \Re^{9 \times 9}$

Then, the Lagrange multipliers can be formulated from Equation (17) since the last six rows of U_s and $\hat{f}_{1,s}$ are null, i.e.

$$\lambda_s = \begin{bmatrix} J_{\Gamma 2,s} \\ J_{\Gamma 3,s} \end{bmatrix}^{-1} \begin{bmatrix} \hat{M}_{12,s}^T & \hat{M}_{22,s} & 0 \\ 0 & 0 & \hat{M}_{33,s} \end{bmatrix} \ddot{q}_c \tag{18}$$

and the three control inputs to the actuators are given by:

$$\begin{bmatrix} u_{1,s} \\ u_{2,s} \\ u_{3,s} \end{bmatrix} = [\hat{M}_{11,s} \;\; \hat{M}_{12,s} \;\; 0] \ddot{q}_c + \hat{f}_{1,s} - J_{\Gamma 1,s} \lambda_s \tag{19}$$

Substituting the control inputs, given by Equation (17), into Equation (13), the error equation of the slow time-scale subsystem is formulated as:

https://doi.org/10.1017/S0263574720004265 Published online by Cambridge University Press

$$\boldsymbol{M}_s\ddot{\boldsymbol{q}}_s = -\boldsymbol{f}_{1,s} + \hat{\boldsymbol{M}}_s\{\ddot{\boldsymbol{q}}_d + \boldsymbol{K}_{sp}(\boldsymbol{q}_d - \boldsymbol{q}) + \boldsymbol{K}_{sd}(\dot{\boldsymbol{q}}_d - \boldsymbol{q})\} + \boldsymbol{f}_{1,s} \quad (20)$$

Rewriting the Equation (20),

$$(\ddot{\boldsymbol{q}}_d - \ddot{\boldsymbol{q}}) + \boldsymbol{K}_{sd}(\dot{\boldsymbol{q}}_d - \dot{\boldsymbol{q}}) + \boldsymbol{K}_{sp}(\boldsymbol{q}_d - \boldsymbol{q}) = \hat{\boldsymbol{M}}_s^{-1}\{(\boldsymbol{f}_{1,s} - \hat{\boldsymbol{f}}_{1,s}) + (\boldsymbol{M}_s - \hat{\boldsymbol{M}}_s)\ddot{\boldsymbol{q}}\} \quad (21)$$

If the dynamic parameters are known exactly, i.e. $\hat{\boldsymbol{M}}_s = \boldsymbol{M}_s$ and $\hat{\boldsymbol{f}}_{1,s} = \boldsymbol{f}_{1,s}$, then the right-hand side of Equation (21) is identically zero, and the slow time-scale subsystem is asymptotically stable. However, the mismatch between actual and modeled parameters will cause servo errors to be excited in a complex way, as seen by Equation (21).[19]

With the fast time-scale system state vector defined as:

$$\boldsymbol{X}_f \equiv \begin{bmatrix} z_f \\ z_f' \end{bmatrix} \in \Re^{6r} \quad (22)$$

equations of motion for the fast time-scale subsystem are formulated from Equation (16) as:

$$\dot{\boldsymbol{X}}_f = \boldsymbol{A}\boldsymbol{X}_f + \boldsymbol{B}\boldsymbol{U}_f \quad (23)$$

where: $\boldsymbol{A} = \begin{bmatrix} \boldsymbol{0} & \boldsymbol{I} \\ -\tilde{\boldsymbol{K}}\boldsymbol{H}_{22,s} & \boldsymbol{0} \end{bmatrix} \in \Re^{6r\times 6r}$

$$\boldsymbol{B} = \begin{bmatrix} \boldsymbol{0} \\ -\tilde{\boldsymbol{K}}\boldsymbol{H}_{21,s} \end{bmatrix} \in \Re^{6r\times 9}$$

$$\boldsymbol{U}_f = [u_{f1}\ u_{f2}\ u_{f3}\ 0\ \cdots\ 0]^T \in \Re^9$$

Since the open loop system, described in Equation (23), has r conjugate pairs of poles on the imaginary axis, located at the square root of the corresponding natural frequency, an appropriate damping can be provided by either pole placement or optimal control methods to yield

$$\begin{bmatrix} u_{f1} \\ u_{f2} \\ u_{f3} \end{bmatrix} = -\boldsymbol{K}_f\boldsymbol{X}_f \quad (24)$$

where: $\boldsymbol{K}_f \equiv$ feedback gain matrix for fast time-scale states, $\boldsymbol{K}_f \in \Re^{3\times 6r}$.

From Equations (17) and (24), the composite control scheme has the form:

$$\boldsymbol{U} = \boldsymbol{U}_s(\boldsymbol{q}_s, \dot{\boldsymbol{q}}_s) + \boldsymbol{U}_f(z_f, z_f') \quad (25)$$

5. SIMULATION RESULTS

Simulations were performed to investigate the dynamic characteristics of the flexible link planar parallel manipulator, represented by Equation (6), and the effectiveness of the two-time scale control scheme given by Equation (25). A prototype, similar to the planar parallel manipulator shown in Figure 1, is currently being developed, consequently, physical parameters for the simulation are chosen to have same values as the prototype, and are listed in Table I. Stiffness of linkages used for simulations, *EI*, are far lower than for typical construction materials, to more readily investigate the composite control performance of the planar parallel manipulator. Linear motors actuate the sliders along linear paths.

Table I. Physical parameters of the manipulator used for simulations.

	Parameter	Value
Platform	Mass (m_p)	0.2 kg
	Moment of inertia (I_p)	0.000167 kg m^2
	Side length	0.1 m
Linkage	Mass (m)	0.25 kg
	Length (l)	0.2 m
	Stiffness (EI)	0.021 Nm^2
Slider	Mass (m_s)	0.2 kg
	Stroke	0.4 m
	Angle (α_i)	120°, 270°, 30°

A Cartesian trajectory is selected as given below, as the desired trajectory;

$$x_P = \frac{x_f}{t_f}t - \frac{x_f}{2\pi}\sin\left(\frac{2\pi}{t_f}t\right) \quad (26)$$

The desired trajectory exhibits smooth acceleration, as shown in Figure 4. The platform is positioned at $x=0$, $y=0$ initially with the orientation of 10° in the X-Y plane. The Y-direction and the orientation of the platform are commanded to keep their initial coordinates, i.e. $y=0$ and $\phi=10°$ respectively, while the platform follows the X-direction Cartesian trajectory. Since the desired trajectories of platform are defined in Cartesian coordinates, desired trajectories for actuators to follow, $\boldsymbol{\rho}_d$, are calculated from Cartesian coordinates of the platform through the inverse kinematics of the planar parallel manipulator.[2] With reference to electronic component assembly processes, a typical motion required for the platform is to move 20 mm along the X-axis, as shown in Figure 2, within 0.3 sec.

Three identical links have the first three natural frequencies at 16, 51, 106 rad/s. hence, for the linkage

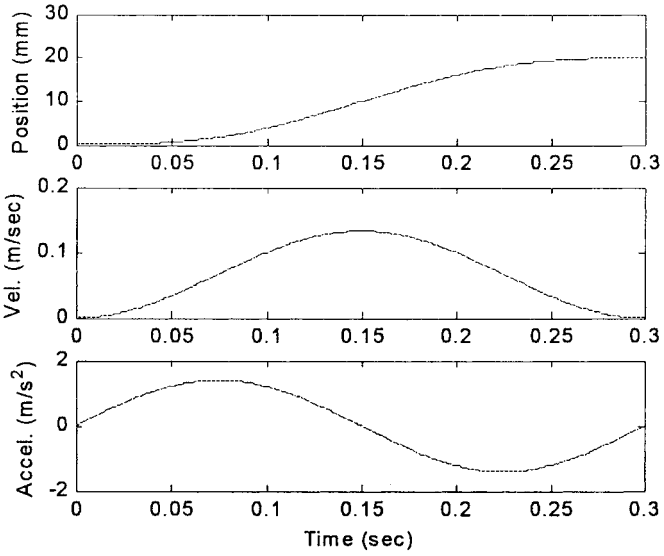


Fig. 4. Desired Trajectory.

https://doi.org/10.1017/S0263574720004265 Published online by Cambridge University Press

selected, $\mu=0.065$, which is sufficiently small to permit separation of the fast time-scale subsystem dynamics from the slow time-scale system dynamics. Assuming perfect knowledge of dynamic parameters in Equation (17), poles of the characteristic equation of the slow time-scale control system, represented by Equation (21) should be located sufficiently far from the first natural frequency of the links, specifically 16 rad/sec., to maintain the separation between the slow time-scale and the fast time-scale. Therefore, diagonal elements of the feedback gain matrices of the slow time-scale controller, $\boldsymbol{K}_{sp}$ and $\boldsymbol{K}_{sd}$ are chosen as 100 and 20 respectively, so that the closed-loop poles of the slow time-scale system are located at $s=-10$ rad/s.

The first two vibration modes are considered in modeling the structural flexibility of three linkages, given by Equation (3), i.e. $r=2$. Results for two cases are presented; the slow time-scale controller alone, given by Equation (19), and the composite controller given by Equation (25). Since the slow time-scale controller alone is designed only for the rigid-body dynamics of the manipulator, performance comparison between two controllers readily illustrates the feasibility of the composite controller in damping structural vibration of the planar parallel manipulator linkages. A fourth order Runge-Kutta integration algorithm was used to integrate the ordinary differential equations given by Equation (8), with the control input applied, given by Equation (25) at an integration interval of 1 msec, using MATLAB™ software.

Feedback gains for the fast time-scale controller are calculated with dynamic parameters obtained for a platform configuration of $x_f=0.02$ m, $y_f=0$ m, $\phi=10°$. Using the linear-quadratic (LQ) state-feedback regulator method, the following gain, $\boldsymbol{K}_f$, was computed, using weighting matrices $\boldsymbol{Q}=\boldsymbol{I}\in\Re^{12\times12}$ and $\boldsymbol{R}=\mathbf{0.1}\boldsymbol{I}\in\Re^{3\times3}$:

$$\boldsymbol{K}_f=\begin{bmatrix} -1 & -1.6 & 0 & 0 & 0 & 0 & 3.3 & -3.2 & 0 & 0 & 0 & 0 \\ 0 & 0 & 0.5 & 0.7 & 0 & 0 & 0 & 0 & -3.3 & 3.2 & 0 & 0 \\ 0 & 0 & 0 & 0 & -1 & -1.6 & 0 & 0 & 0 & 0 & 3.3 & -3.2 \end{bmatrix}$$

As the configuration of the manipulator changes to follow the given trajectory, dynamic parameters making up the state-space matrices, $\boldsymbol{A}$ and $\boldsymbol{B}$, in Equation (23), vary along the trajectory, that eventually leads to different optimal gains for the fast time-scale system along the trajectories to follow. Since planar parallel manipulators usually undergo small repetitive motions in an electronic component assembly processes, dynamic parameters do not vary significantly with motion of only 0.02 m. Hence, the terminal coordinates of the trajectory, i.e. $x=0.02$ m, $y=0$ m, $\phi=10°$, were used to calculated the optimal feedback gains for the fast time-scale system.

Figure 5 shows X-directional trajectories of the platform at its mass center. Since the slow time-scale controller alone is designed to compensate only for the rigid-body model, its tracking exhibits persistent oscillation. In contrast, the composite controller damped out structural vibration after two seconds. The Y-directional movement and the orientation of the platform are shown in Figure 6. These coordinates are to maintain their initial values, i.e. $y_p=0$ m and $\phi=10°$, respectively. The Y-directional movements of the platform exhibit similar oscillations in both two cases, while the composite controller yields a faster settling time for the orientation of the platform than the slow time-scale controller alone. Figure 7, showing flexible deformations of the linkages at the distal end of the linkages, C_i, reveals that the composite controller damps out structural vibration of the linkages as expected. The first two vibration modes of the third linkage are shown in Figure 8. Since the first two vibration modes are included in modeling the structural flexibility, given by Equation (3), and are controlled by the optimal feedback controller, $\boldsymbol{K}_f$, they are damped out effectively.

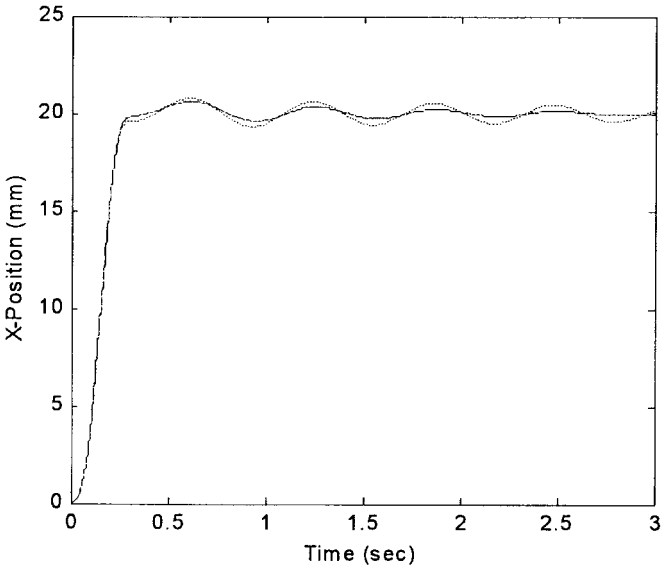


Fig. 5. X-directional tracking performance (solid line: composite controller, dotted line: slow time-scale controller alone).

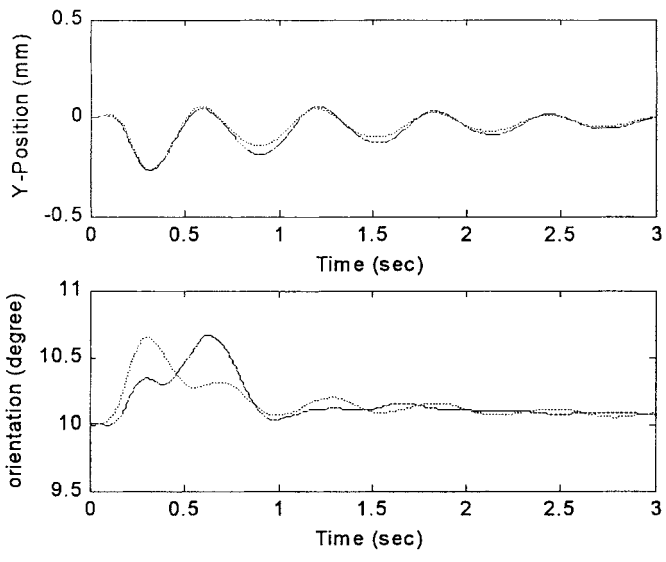


Fig. 6. Y-directional movement and orientation of the platform (solid line: composite controller, dotted line: slow time-scale controller alone).

https://doi.org/10.1017/S0263574720004265 Published online by Cambridge University Press

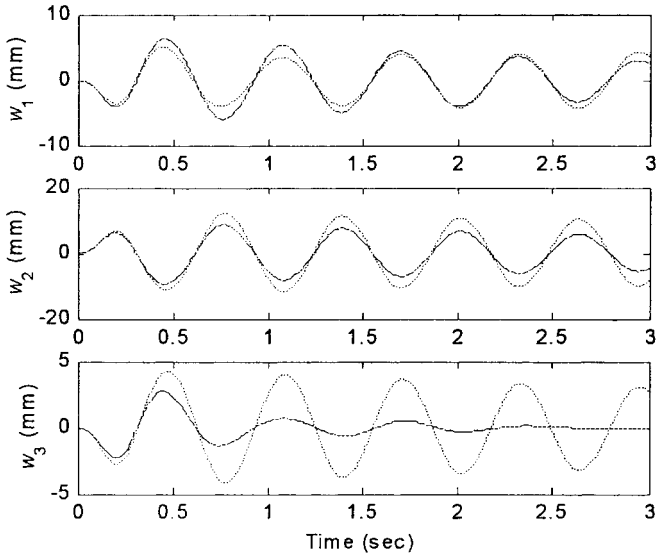


Fig. 7. Flexible deformation of each link at C_i
(solid line: composite controller, dotted line: slow time-scale controller alone).

When designing the fast time-scale controller, given by Equation (24), poles of the closed-loop system were shifted from $s=\pm 4j$, $s=\pm 13j$ to $s=-0.27\pm 3.99j$ and $s=-1.49\pm 12.87j$ by the action ofthe feedback controller, $\boldsymbol{K}_f$. Considering only the dominant poles, located at $s=-0.27\pm 3.99j$, the open loop system was altered with feedback, to an under-damped system, with a damping ratio of 0.1. Hence, since the damping of the closed-loop system is not large enough to achieve rapid attenuation of structural vibration, several seconds must elapse prior to the vibration effectively being damped. This is shown in Figure 5 and Figure 6. Note the use of large feedback gains to increase the damping ratio further, may result in poles of the closed-loop system shifted far from the imaginary axis may cause instability of the closed-loop system. Figure 9 illustrates that the fast time-scale controller generates a control input which is substantially smaller than the slow time-scale or rigid body controller.

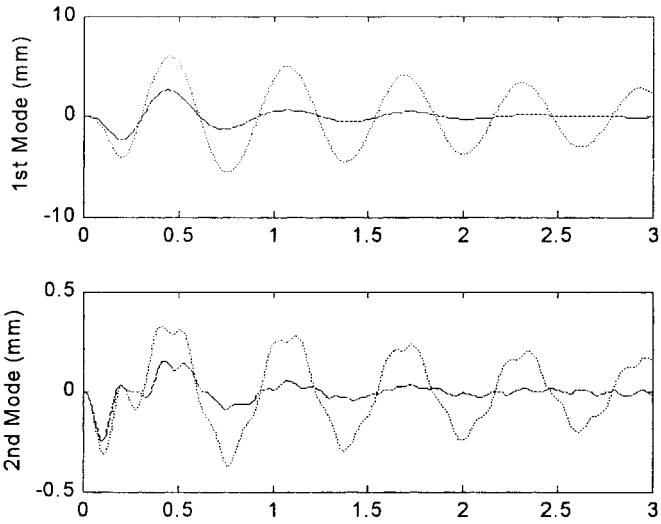


Fig. 8. Time response of first two modes of the third link
(solid line: composite controller, dotted line: slow time-scale controller alone).

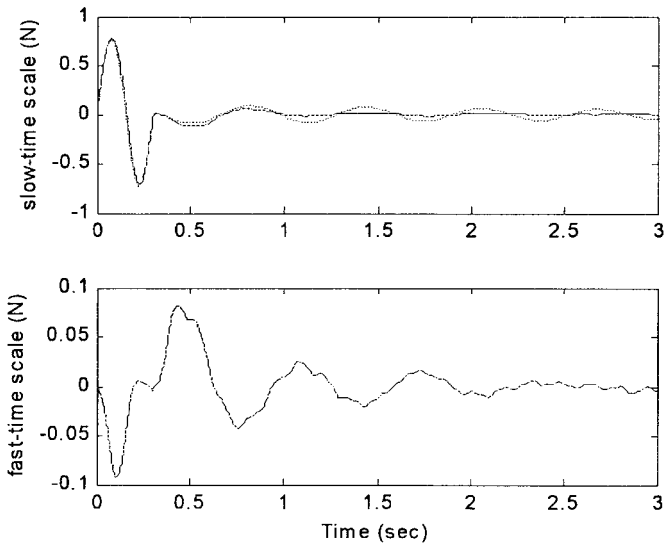


Fig. 9. Control input for actuators (third link)
(solid line: composite controller, dotted line: slow time-scale controller alone).

6. CONCLUSION

A two-time scale controller design approach is proposed for a planar parallel manipulator with the structurally flexible linkages. In the composite controller, the slow time-scale control scheme is formulated to follow a desired motion trajectory using a computed torque controller, and the fast time-scale control scheme is designed to damp the vibration of flexible linkages arising from rapid rigid-body motions of the manipulator using a linear quadratic state-feedback regulator. Simulation results demonstrate that the composite control scheme yields good damping performance of structural vibrations and precise manipulation of the platform despite multiple closedloop chains with structural flexible elements, which interfere with each other. The application of this composite control demonstrates the feasibility of such a controller, applied to a planar parallel manipulator with lightweight linkages.

References

1. C. Gosselin and J. Angeles, "The Optimum Kinematic Design of a Planar Three-Degree-of-Freedom Parallel Manipulator", *ASMV J. Mechanisms, Transmissions, and Automation in Design* **110**(1), 35–41 (1998).
2. C. M. Gosselin, S. Lemieux, and J.-P. Merlet, "A New Architecture of Planar Three-Degree-of-Freedom Parallel Manipulator", *Proc. IEEE Int. Conference on Robotics and Automation*, Minneapolis, Minnesota (1996) pp. 3738–3743.
3. S. Kock and W. Schmacher, "A Parallel X-Y Manipulator With Actuation Redundancy For High-Speed And Active-Stiffness Applications", *Proc. IEEE Int. Conference on Robotics and Automation*, Leuven, Belgium (1998) pp. 2295–2300.
4. J.-P. Merlet, "Direct Kinematics of Planar Parallel Manipulators", *Proc. IEEE Int. Conference on Robotics and Automation*, Minneapolis, Minnesota (1996) pp. 3744–3749.
5. C. Gosselin and J. Angeles, "Singularity Analysis of Closed-Loop Kinematic Chains", *IEEE Trans. on Robotics and Automation* **6**(3), 281–290 (1990).
6. I. A. Bonov and C. M. Gosselin, "Singularity Loci of Planar Parallel Manipulators With Revolute Joints", *Proc. 2nd Workshop on Computational Kinematics (CK2001)*, Seoul, South Korea (2001) pp. 291–299.

https://doi.org/10.1017/S0263574720004265 Published online by Cambridge University Press

7. W. Q. D. Do and D. C. H. Yang, "Inverse Dynamic Analysis and Simulation of a Platform Type of Robot", *J. Robotic Systems* **5**(3), 209–227 (1988).
8. H. Pang and M. Shahinpoor, "Inverse Dynamics of a Parallel Manipulator", *J. Robotic Systems* **11**(8), 693–702 (1994).
9. B.-S. Yuan, J. W. Lee and W. J. Book, "Dynamic Analysis and Control of Lightweight Arms With a Parallel Mechanism", *Proc. USA-Japan Symp on Flexible Automation – Crossing Bridges: Advanced Flexible Automation and Robotics*, Minneapolis, Minnesota (1988) pp. 369–374.
10. A. Fattah, J. Angeles and A. K. Misra, "Dynamic of a 3-DOF Spatial Parallel Manipulator With Flexible Links", *Proc. IEEE Int. Conference on Robotics and Automation*, Nagoya, Japan (1995) pp. 627–632.
11. B. Kang and J. K. Mills, "Dynamic Modeling and Vibration Control of High Speed Planar Parallel Manipulator", *Proc. IEEE/RSJ Int. Conference on Intelligent Robots and Systems*, Maui, Hawaii (2001) pp. 1287–1292.
12. B. Siciliano and W. J. Book "A Singular Perturbation Approach To Control of Lightweight Flexible Manipulators", *J. Robotics Research* **7**(4), 79–90 (1988).
13. B. Siciliano, J. V. R. Prasad and A. J. Calise, "Output Feedback Two-Time Scale Control of Multilink Flexible Arms", *ASME Journal of Dynamic Systems and Measurement, and Control* **114**, 70–77 (1992).
14. B. Siciliano and L. Villani, "Two-Time Scale Force and Position Control of Flexible Manipulators", *Proc. IEEE Int. Conference on Robotics and Automation*, Seoul, South Korea (2001) pp. 2729–2739.
15. F. Matsuno and K. Yamamoto, "Dynamic Hybrid Position/Force Control of a Flexible Manipulator", *Proc. IEEE Int. Conference on Robotics and Automation*, Atlanta, Georgia, NJ (1993) pp 462–467.
16. D. Stewart, "A Platform With Six Degrees of Freedom", *Proc. Institution of Mechanical Engineers* **180**(5), 371–378 (1965).
17. G. Genta, *Vibration of Structures and Machines* (Springer-Verlag, New York, 1993).
18. P. K. Khosla and T. Kanade, "Real-Time Implementation and Evaluation of Computed Torque Scheme", *IEEE Trans. on Robotics and Automation* **5**(2), 245–253 (1989).
19. J. J. Craig, *Introduction to Robotics* (Addison-Wesley Publishing Company, 1986).

APPENDIX

$m_p \equiv$ mass of the platform
$I_p \equiv$ mass moment of inertia of the platform at the mass center
$m_s \equiv$ mass of the slider
$m \equiv$ mass of linkages
$l \equiv$ length of linkages
$E \equiv$ Young's modulus of linkages
$I \equiv$ area moment of inertia of linkages

$$\boldsymbol{M}_{11} = (m_s + m)\begin{bmatrix} 1 & 0 & 0 \\ 0 & 1 & 0 \\ 0 & 0 & 1 \end{bmatrix} \in \Re^{3\times 3} \qquad \boldsymbol{M}_{12} = \frac{ml}{2}\begin{bmatrix} s_1 & 0 & 0 \\ 0 & s_2 & 0 \\ 0 & 0 & s_3 \end{bmatrix} \in \Re^{3\times 3}$$

$$\boldsymbol{M}_{14} = m\begin{bmatrix} s_1\int\psi_1 d\xi & \cdots & s_1\int\psi_r d\xi & 0 & \cdots & 0 & 0 & \cdots & 0 \\ 0 & \cdots & 0 & s_2\int\psi_1 d\xi & \cdots & s_2\int\psi_r d\xi & 0 & \cdots & 0 \\ 0 & \cdots & 0 & 0 & \cdots & 0 & s_3\int\psi_1 d\xi & \cdots & s_3\int\psi_r d\xi \end{bmatrix} \in \Re^{3\times 3r}$$

$$\boldsymbol{M}_{22} = \frac{ml^2}{3}\begin{bmatrix} 1 & 0 & 0 \\ 0 & 1 & 0 \\ 0 & 0 & 1 \end{bmatrix} \in \Re^{3\times 3} \qquad \boldsymbol{M}_{33} = \begin{bmatrix} m_p & 0 & 0 \\ 0 & m_p & 0 \\ 0 & 0 & I_p \end{bmatrix} \in \Re^{3\times 3}$$

$$\boldsymbol{M}_{24} = ml\begin{bmatrix} \int\psi_1\xi d\xi & \cdots & \int\psi_r\xi d\xi & 0 & \cdots & 0 & 0 & \cdots & 0 \\ 0 & \cdots & 0 & \int\psi_1\xi d\xi & \cdots & \int\psi_r\xi d\xi & 0 & \cdots & 0 \\ 0 & \cdots & 0 & 0 & \cdots & 0 & \int\psi_1\xi d\xi & \cdots & \int\psi_r\xi d\xi \end{bmatrix} \in \Re^{3\times 3r}$$

$$\boldsymbol{M}_{44} = m\begin{bmatrix} \hat{\boldsymbol{M}} & \boldsymbol{0} & \boldsymbol{0} \\ \boldsymbol{0} & \hat{\boldsymbol{M}} & \boldsymbol{0} \\ \boldsymbol{0} & \boldsymbol{0} & \hat{\boldsymbol{M}} \end{bmatrix} \in \Re^{3r\times 3r} \qquad \hat{\boldsymbol{M}} = \begin{bmatrix} \int\psi_1^2 d\xi & \cdots & 0 \\ \vdots & \cdots & \vdots \\ 0 & \cdots & \int\psi_r^2 d\xi \end{bmatrix} \in \Re^{r\times r}$$

https://doi.org/10.1017/S0263574720004265 Published online by Cambridge University Press

$$\boldsymbol{K}=\frac{EI}{l^3}\begin{bmatrix}\hat{\boldsymbol{K}} & \boldsymbol{0} & \boldsymbol{0}\\ \boldsymbol{0} & \hat{\boldsymbol{K}} & \boldsymbol{0}\\ \boldsymbol{0} & \boldsymbol{0} & \hat{\boldsymbol{K}}\end{bmatrix}\in\Re^{3r\times 3r} \qquad \hat{\boldsymbol{K}}=\begin{bmatrix}\int\left(\frac{\mathrm{d}^2\psi_1}{d\xi^2}\right)^2\mathrm{d}\xi & \cdots & 0\\ \vdots & \cdots & \vdots\\ 0 & \cdots & \int\left(\frac{\mathrm{d}^2\psi_2}{d\xi^2}\right)^2\mathrm{d}\xi\end{bmatrix}\in\Re^{r\times r}$$

$$\boldsymbol{V}_1=-m\begin{bmatrix}0.5lc_1\dot{\beta}_1^2+\sum_{j=1}^{r}\dot{\eta}_{1j}\dot{\beta}_1c_1\int\psi_j d\xi\\ 0.5\mathrm{l}c_2\dot{\beta}_2^2+\sum_{j=1}^{r}\dot{\eta}_{2j}\dot{\beta}_2c_2\int\psi_j d\xi\\ 0.5\mathrm{l}c_3\dot{\beta}_3^2+\sum_{j=1}^{r}\dot{\eta}_{3j}\dot{\beta}_3c_3\int\psi_j d\xi\end{bmatrix}\in\Re^3 \qquad \boldsymbol{V}_2=m\begin{bmatrix}\sum_{j=1}^{r}\dot{\eta}_{1j}\dot{\rho}_1c_1\int\psi_j d\xi\\ \sum_{j=1}^{r}\dot{\eta}_{2j}\dot{\rho}_2c_2\int\psi_j d\xi\\ \sum_{j=1}^{r}\dot{\eta}_{3j}\dot{\rho}_3c_3\int\psi_j d\xi\end{bmatrix}\in\Re^3$$

$$\boldsymbol{V}_4=-m\begin{bmatrix}c_1\dot{\rho}_1\dot{\beta}_1\int\psi_1 d\xi\\ \vdots\\ c_1\dot{\rho}_1\dot{\beta}_1\int\psi_r d\xi\\ c_2\dot{\rho}_2\dot{\beta}_2\int\psi_1 d\xi\\ \vdots\\ c_2\dot{\rho}_2\dot{\beta}_2\int\psi_r d\xi\\ c_3\dot{\rho}_3\dot{\beta}_3\int\psi_1 d\xi\\ \vdots\\ c_3\dot{\rho}_3\dot{\beta}_3\int\psi_r d\xi\end{bmatrix}\in\Re^{3r}$$

where: $s_i\equiv\sin(\alpha_i-\beta_i)\qquad i=1,2,3$

$c_i\equiv\cos(\alpha_i-\beta_i)\qquad i=1,2,3$

$$\boldsymbol{J}_{\Gamma 1}=\begin{bmatrix}\cos\alpha_1 & \sin\alpha_1 & 0 & 0 & 0 & 0\\ 0 & 0 & \cos\alpha_2 & \sin\alpha 2 & 0 & 0\\ 0 & 0 & 0 & 0 & \cos\alpha_3 & \sin\alpha_3\end{bmatrix}\in\Re^{3\times 6}$$

$$\boldsymbol{J}_{\Gamma 2}=\begin{bmatrix}s2_1 & c2_1 & 0 & 0 & 0 & 0\\ 0 & 0 & s2_2 & c2_2 & 0 & 0\\ 0 & 0 & 0 & 0 & s2_3 & \mathrm{c}2_3\end{bmatrix}\in\Re^{3\times 6}$$

where: $s2_i\equiv -l\sin\beta_i-\cos\beta_i\sum_{j=1}^{r}\eta_{ij}\qquad i=1,2,3$

$c2_i\equiv l\cos\beta_i-\sin\beta_i\sum_{j=1}^{r}\eta_{ij}\qquad i=1,2,3$

$$\boldsymbol{J}_{\Gamma 3}=\begin{bmatrix}-1 & 0 & -1 & 0 & -1 & 0\\ 0 & -1 & 0 & -1 & 0 & -1\\ \mathrm{s}3_1 & -c3_1 & s3_2 & -c3_2 & s3_3 & -c3_3\end{bmatrix}\in\Re^{3\times 6}$$

where: $s3_i\equiv l_{C_i}\sin(\phi_i+\phi)\qquad i=1,2,3$

$c3_i\equiv l_{C_i}\cos(\phi_i+\phi)\qquad i=1,2,3$

$l_{C_i}\equiv$ distance from the mass center, P, to the i^{th} vertex of the platform, C_i

$\phi_1,\ \phi_2,\ \phi_3\equiv 150°,\ 270°,\ 30°$ respectively.

https://doi.org/10.1017/S0263574720004265 Published online by Cambridge University Press

$$\boldsymbol{J}_{\Gamma 4}\begin{bmatrix} -\sin\beta_1 & \cos\beta_1 & & & & \\ \vdots & \vdots & 0 & & 0 & \\ -\sin\beta_1 & \cos\beta_1 & & & & \\ & & -\sin\beta_2 & \cos\beta_2 & & \\ 0 & & \vdots & \vdots & 0 & \\ & & -\sin\beta_2 & \cos\beta_2 & & \\ & & & & -\sin\beta_3 & \cos\beta_3 \\ 0 & & 0 & & \vdots & \vdots \\ & & & & -\sin\beta_3 & \cos\beta_3 \end{bmatrix} \in \Re^{3r\times 6}$$

https://doi.org/10.1017/S0263574720004265 Published online by Cambridge University Press